Transparent conductive PEDOT–graphene films from large-flake graphite

Sean T. McDermott[†], Brenden Ferland[†], Jinzhou Liu[†], Prabodha Abeykoon[‡], Michael J. Joyce[‡], Seth Shuster[‡], Steven L. Suib[‡,#,§] Douglas H. Adamson[†,‡,*]

† Polymer Program, Institute of Materials Science, University of Connecticut, Storrs CT 06269

‡ Department of Chemistry, University of Connecticut, Storrs CT 06269

Institute of Materials Science, University of Connecticut, Storrs, CT 06269

§ Department of Chemical and Biomolecular Engineering, University of Connecticut, Storrs, CT 06269

Keywords: Two-dimensional materials, Solvent interface trapping, Conductive polymers, PEDOT: graphene, Sensor

The demand for affordable, flexible, transparent, and robust thin film electrodes in organic electronics has highlighted the limitations of indium tin oxide (ITO), which suffers from fragility and high costs. Poly(3,4-ethylenedioxythiophene) (PEDOT), particularly when doped with poly(styrene sulfonate) (PSS), has emerged as a promising alternative due to its mechanical flexibility, electrical conductivity, and environmental stability. However, PSS's insulating nature, hygroscopicity, and acidity present significant drawbacks. This study explores an alternative approach using large-flake graphene, exfoliated through a solvent interface trapping method (SITM), as a dopant for PEDOT. The resulting PEDOT-graphene films exhibit conductivities reaching 1070 S/cm, surpassing those of previously reported PEDOT-based films. The graphene sheets, acting as templates during vapor-phase polymerization (VPP) of PEDOT, enhance the film's conductivity by increasing electron pathways and crystalline regions within PEDOT. Characterization through SEM, TEM, XRD, Raman spectroscopy, XPS, and UV-Vis spectroscopy confirms the structural and electrical integrity of the films. Additionally, these films demonstrate potential applications in sensing technologies, particularly responsive to volatile organic compounds such as triethylamine. This work presents a scalable method for producing high-conductivity, transparent PEDOT-graphene films, offering a viable alternative to ITO in organic electronic applications.

INTRODUCTION

The field of organic electronics requires affordable, flexible, transparent, and robust thin film electrodes to replace the current industry standard of indium tin oxide (ITO)—a substance plagued by its fragility and high cost.[1] Important candidates for ITO replacement are semiconducting polymers[2–4] due to their mechanical flexibility, electrical conductivity, and conformability. These properties enable many applications in organic electronics, such as sensors, supercapacitors, and solar cells.[5–12] Poly(3,4-ethylenedioxythiophene) (PEDOT) has emerged as a promising candidate due to its superior electronic and ionic conductivities, desirable optical properties, and resistance to humidity and oxidants.[13] However, PEDOT is insoluble in most organic and aqueous solvents, so it is typically combined with PSS, allowing PEDOT to be dispersed in aqueous solutions to enhance its processability.[14] Additionally, PSS serves as a dopant, and the presence of PSS has been shown to result in a more crystalline PEDOT structure.[15,16]

Unfortunately, PSS also has its drawbacks. It is an insulator that can potentially limit PEDOT's conductivity,[14 17] it is acidic, and can lead to material incompatibility issues, and the thermal stability of PSS is such that it can limit the processing options for manufacturing. Thus, in many applications, PEDOT: PSS films must undergo

post-treatment to remove the PSS. To address these challenges, we used films of overlapping large-flake graphene exfoliated through solvent interface trapping as a dopant for PEDOT. We synthesized PEDOT–graphene films with conductivities reaching 1070 S/cm, surpassing those of comparable films previously reported.

In addition to being a dopant, graphene's other unique properties present a compelling case for its use with PEDOT.[18] Other dopants, such as sulfuric acid and organic acids, have been investigated.[19,20] However, unlike small-molecule dopants, graphene is non-volatile, does not leach, and is electrically conductive. Yet the production of high-quality graphene remains challenging. Chemical vapor deposition (CVD) and micromechanical exfoliation can produce relatively defect-free graphene but are limited to only one graphene sheet at a time.[21,22] Other, more scalable methods tend to produce materials with defects that lower electrical conductivity and degrade desirable properties.[23] The most common example of such a method is the reduction of graphene oxide (GO).[24,25] This technique allows for the scalable production of reduced graphene oxide (rGO). However, this method creates holes and defects in the graphene hexagonal carbon matrix. These defects interrupt the percolating network of the graphene and lower its conductivity.[26,27]

Liquid exfoliation is an alternative, scalable method. This approach utilizes high-boiling organic solvents such as *N*-methyl-2-pyrrolidone (NMP). NMP stabilizes graphene suspensions, slowing restacking and sedimentation.[28] Exfoliation is accomplished by tip sonication, and the resulting suspension of graphene is centrifuged to remove the unexfoliated material.[29,30] Although the approach provides relatively large-scale production, removing these high-boiling solvents requires high energy and time. Furthermore, recent studies have shown that the ultrasonication of solvents can produce graphene-like quantum dots and damage the hexagonal structure of graphene,[31–33] introducing doubt about the integrity of the produced graphene.

For this study, we modified the solvent interfacial trapping method (SITM) to address these challenges, offering a convenient approach for the scalable production of graphene. The approach takes advantage of the high interfacial energy between water and oil and the insolubility of graphene in both.[34] The addition of graphite to a mixture of oil and water leads to the graphite being pinned at the oil-water interface. The graphite spontaneously exfoliates at the interface, as the spreading graphene sheets act as surfactants and lower the system's free energy.[35] When this system is shaken, it increases the area of the oil-water interface, forming graphene-stabilized emulsions.[36,37] With this approach, conductive transparent films of pristine graphene can be quickly and inexpensively produced.[34]

The challenge comes with large flake graphite. In a previous study, we found that the rate of exfoliation is inversely proportional to the size of the graphite flakes, with larger flakes requiring a significantly longer exfoliation time.[38] Since we hypothesized that larger graphene sheet sizes would maximize the conductivity of our films, we developed an improved approach for exfoliating large flake-size graphite without resorting to high-energy sonication, which can lead to defects in the graphene.

In this work, we used a film of overlapping graphene sheets as a template for PEDOT's vapor-phase polymerization (VPP). Graphene is known to π-π stack with itself and other materials, increasing the connected electron pathways and crystalline regions within PEDOT.[39] With this approach, we synthesized PEDOT–graphene films with conductivities greater than 1070 S/cm.

EXPERIMENTAL

Materials

Graphite samples were obtained from Asbury Carbon (Asbury, NJ). Ethyl alcohol (Acros, reagent grade), iron(III) *p*-toluenesulfonate hexahydrate (Aldrich, technical grade), 1-butanol (Fisher, certified ACS), heptane (Fisher, technical grade), triethylamine (Aldrich, ≥ 99%), 3,4-ethylenedioxythiophene (TCI, >98.0%) and trichloro(octadecyl)silane (Aldrich, ≥90%) were used as received.

Exfoliation of graphene

A vial was silanized using trichloro(octadecyl)silane to make it hydrophobic. The hydrophobic vial was charged with approximately 25 mg graphite, 10 mL DI water, and 10 mL heptane. The vial was then bath-sonicated for 30 s. This mixture was then transferred to a centrifuge tube and homogenized using a Silverson Model L5M-A homogenizer at 10,000 rpm for 1 min. Once completed, it was transferred back to the hydrophobic vial and microwaved for 30 s at 30% power using an 1100 W microwave. This mixture was then transferred to a centrifuge tube and homogenized for 1 min. Next, a glass slide was placed in the tube and vortexed for 1 min. It was then removed from the vortex mixer and allowed to equilibrate for 30 s. Finally, the films were removed and air-dried.

Spin coating Iron(III) p-toluenesulfonate hexahydrate

A 40 wt. % Fe(III) *p*-toluenesulfonate hexahydrate ($Fe(OTs)_3$) solution was spin-coated onto the graphene film at 200 rpm for 30 s. This process served to pre-coat the film and facilitate optimal spreading. Subsequently, an additional spin-coating was performed at 1,000 rpm for 30 s. The film was then quickly removed and placed on a hot plate set to 50 °C for 5 minutes to prevent crystallization of the $Fe(OTs)_3$ during drying.[40]

Vapor-phase polymerization of EDOT

EDOT (200 µL) was added to a cotton ball and placed with a stir bar at the bottom of a desiccator. To maintain a constant humidity, the coated graphene film was placed in a desiccator with a water-saturated MgCl solution and a humidity sensor. A vacuum was pulled for 5 min using a membrane pump, and the desiccator was placed on a hot plate at 70 °C for two hours. Subsequently, the film was removed and annealed in an oven at 60 °C. This was then cooled and washed with ethanol to remove any residual oxidant.

Characterization

Electrical measurements were performed on a Signatone S-302 four-point probe, and all sheet resistance measurements were based on an average of at least ten different spots on the film. Scanning Electron Microscopy (SEM) images were captured using an FEI NovaSEM 450. X-ray diffraction (XRD) measurements were performed using a Bruker D2 Phaser Diffractometer. Raman was performed on a 514 nm laser excitation using the Renishaw system 2000. XPS was performed using a K-Alpha Thermo Fisher Scientific XPS instrument, and the spectra were deconvoluted using CasaXPS. UV-Vis spectra were collected using a Perkin Elmer Lambda 1050 instrument. Transmission electron microscopy (TEM) images were captured on a Tecnai 12 D1122 twin using a WAC CCD camera. The sample was mounted on a Quantifoil R 2/2 Copper 400 mesh grid.

RESULTS AND DISCUSSION

The first step in making the PEDOT/graphene films was to create a film of overlapping graphene sheets. To optimize the conductivity of the graphene film, we employed a significantly larger graphite flake size, 300 µm, than conventionally used in the SITM approach. However, the exfoliation of large flake graphite is difficult because of the slow exfoliation kinetics.[38] We overcame this by using vortex mixing, which increased the mixing, and thus the interfacial area, of the oil/water mixture. Since the exfoliation of graphite is driven by decreasing the interfacial energy between oil and water, increasing the area of the interface increased the total number of exfoliation events in the system, increasing the overall rate of exfoliation, even if the exfoliation rate of each event remained relatively slow. This method not only facilitates the production of large graphene sheets but also avoids the need for tip sonication, thereby preserving the large lateral sheet size of the graphene.

The film of overlapping graphene sheets was then formed by placing a glass slide in a vortexed mixture of graphite, water, and oil. The exfoliated graphene climbed the glass slide, separating the heptane vapor from the adsorbed water on the glass slide, creating an overlapping film of graphene sheets that was transparent and electrically conductive.[34] The success of this approach is illustrated in Figure 1A by the Raman spectrum of a graphene film created by graphene climbing a glass slide after vortex mixing. Because the film also contained occasional unexfoliated graphite flakes, the Raman spectra showed a combination of graphene and graphite. The broadening at lower wavenumbers of the film peak relative to the graphite flake peak indicated that a significant portion of the sample was exfoliated to some degree.

We utilized a Raman spectroscopy-based method described by Paton et al. to determine the average stacking of our graphene films.[3] By measuring the intensity ratios of the 2D band peak and its low-energy shoulder for both graphene and graphite samples, we calculated a metric M of 0.681. Applying the empirical formula, $N_L \approx 10^{(0.84M+0.45M^2)}$, we estimated the average degree of stacking in our graphene films to be six layers. Since this average includes occasional unexfoliated graphite flakes, this number of layers is likely significantly smaller away from the flakes.

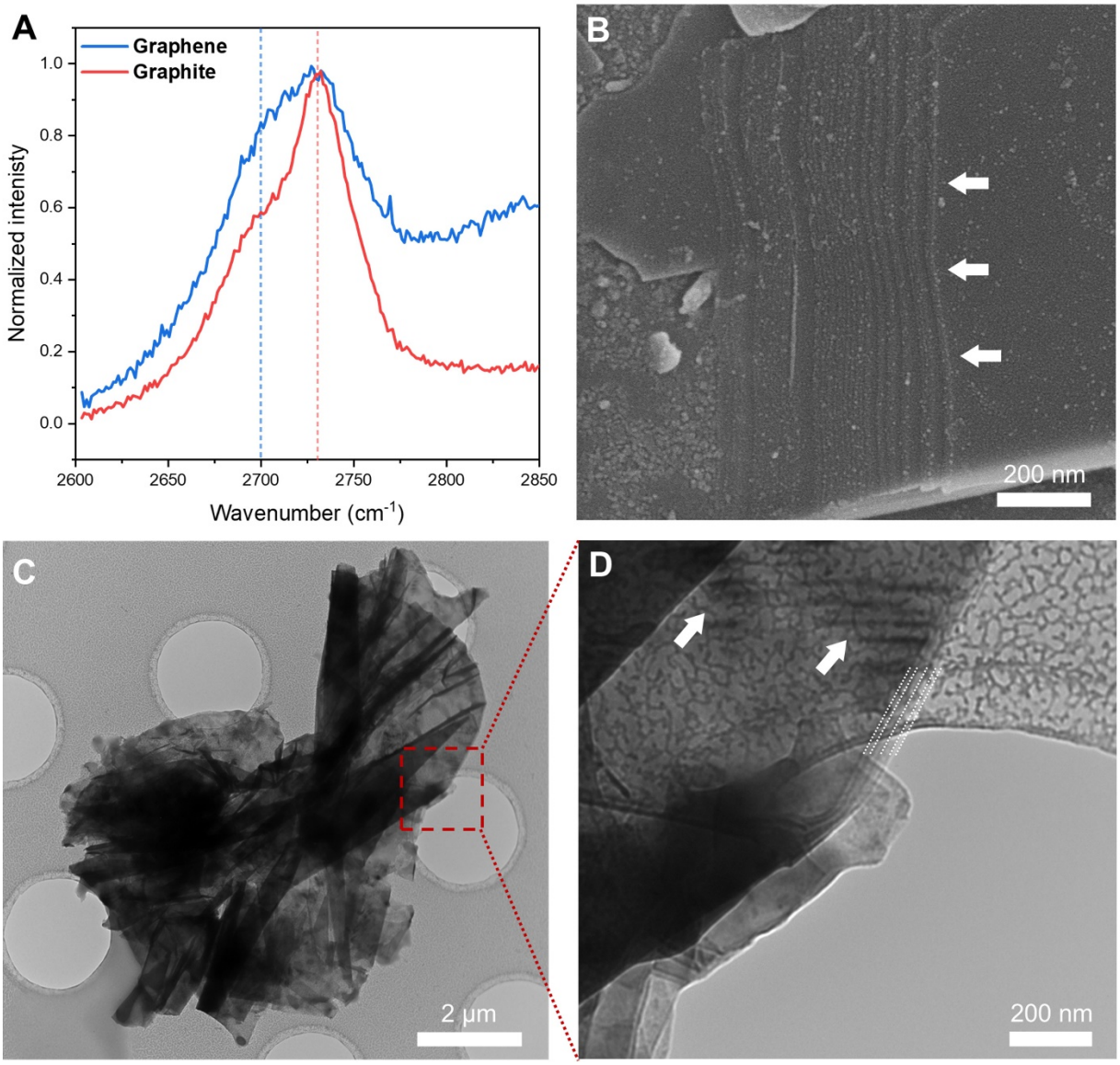

Figure 1. A) Raman spectra of a film of overlapping graphene sheets on a glass slide made using 300 µm flake graphite exfoliated via the SITM method (blue) and 300 µm flake graphite (red). Dotted lines indicate apex (red) and apex - 30 cm^{-1} (blue) used for layer quantification. B) An SEM image of a graphite flake mid-exfoliation with arrows pointing to the first step-edge formed as the graphene sheets slide off the graphite stack, much like playing cards in a ribbon spread. C) TEM image of small partially exfoliated graphite particle. D) Expansion of (C) showing four countable graphene layers in the early stages of exfoliation. Highlighted with arrows are moiré patterns. Dotted lines show countable layers.

SEM imaging, shown in Figure 1B, depicts a graphite flake partly exfoliated, revealing a stepped structure characteristic of incompletely separated graphene layers. These step-like features correspond to the edges of graphene sheets, illustrating a progressive delamination process analogous to the fanning out of cards in a deck. TEM images, shown in Figures 1C and 1D, show an aggregated graphene particle approximately five layers thick. This sample was prepared by pulling a TEM grid through a film of overlapping graphene sheets at a water-heptane interface. The zoomed-in image in Figure 1D provides an approximation of the graphene layer thickness. Moiré patterns indicate the sheets have shifted relative to one another. The average number of layers counted in the TEM image closely agreed with Raman and UV-Vis results.

These films of overlapping graphene sheets formed the basis of our transparent conductive films. They were transparent and conductive on their own, but to increase their conductivity and provide mechanical stability, we

coated them with PEDOT using vapor-phase polymerization (VPP) of EDOT. We hypothesized that the conjugated graphene network would enable EDOT to be templated on the graphene surface to produce highly crystalline PEDOT. The polymerization process is illustrated in Scheme 1.

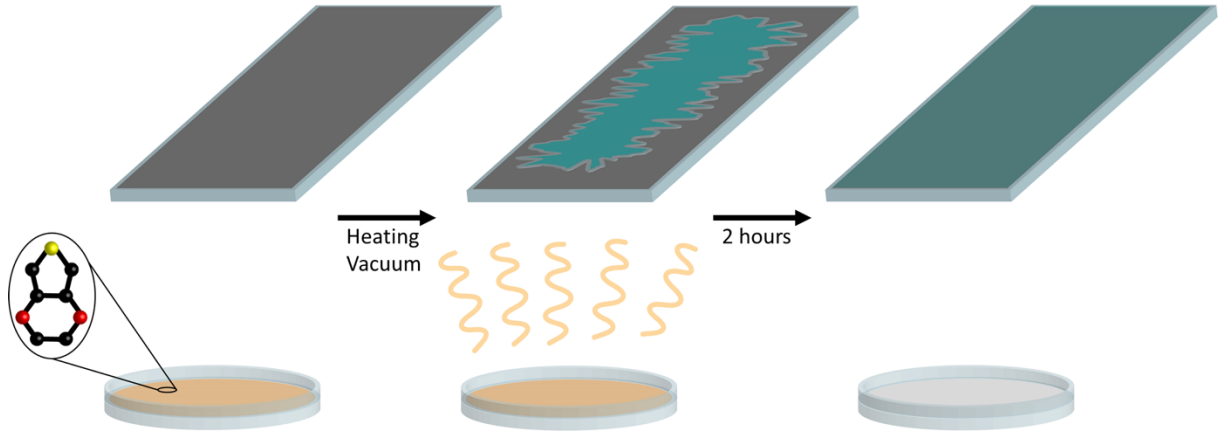

Scheme 1. PEDOT vapor-phase polymerization. The graphene film is spin-coated with the redox reagent, and the EDOT is in a petri dish, vaporized, and then condensed and polymerized on the graphene surface.

First, the graphene film was coated with $Fe(OTs)_3$ via spin coating, which was found to be a superior coating method compared to dip coating. This method required heating during drying to prevent the $Fe(OTs)_3$ from crystallizing,[40] as no polymerization was observed if this redox reagent was allowed to crystallize. Additionally, we found the conductivity was extremely low if the reaction was performed in an arid environment.[40] Therefore, all reactions were conducted in a humidity-controlled environment, achieved by placing a water-saturated solution of $MgCl_2$ in the chamber during the polymerization. This maintained a relative humidity of approximately 36% throughout the polymerization process. A successful polymerization was indicated by the film becoming a light blue color.

XRD, presented in Figure 2A, was utilized to evaluate the orientation and crystallinity of the PEDOT on the graphene film. The XRD spectrum of a film containing just PEDOT is shown in Figure S1. Notably, the characteristic peaks of PEDOT and graphene coincided, indicating that the PEDOT interlayer spacing closely matched the graphene.[20] The spacing was approximately 3.5 Å, indicating lamellar or face-on-stacking of the PEDOT chains; this was the expected result.[41] Also shown in Figure S1 and Figure 2A are the XRD spectra illustrating the effect of sulfuric acid on the PEDOT and PEDOT – graphene film. Sulfuric acid is often used to enhance the conductivity of conductive films. Unfortunately, in our system, the conductivity consistently decreased with the addition of H_2SO_4. A possible explanation for this decrease in conductivity is our observation that the PEDOT underwent a structural change when doped with an acid, delaminating from the graphene surface.[20] This delamination phenomenon may explain why post-treatment of the films permanently lowered their conductivity.

Raman spectroscopy has shown that PEDOT and graphene form π-π stacking between the components.[18] This results from non-covalent π-π interactions between PEDOT's conjugated backbone and graphene's sp^2 carbon lattice, and the parallel alignment of PEDOT's aromatic structure with the graphene surface facilitates π-electron system overlap. Figure S2 compares the Raman shift of our PEDOT-graphene film with that of a control graphene film. Further structural insights are provided by Figure 2B, which presents an SEM image of the PEDOT-graphene film. The image illustrates the composite film's continuous structure, with PEDOT filling the gaps between the graphene sheets. This arrangement contributed to the improved conductivity of the composite.

XPS was performed to confirm the presence of pristine graphene and provide further evidence of the PEDOT's interaction with graphene. These spectra are shown in Figure S3. XPS confirmed the integrity of the graphene during the exfoliation process, as evidenced by the low amount of oxygen functionality in the XPS spectra shown in Figure S3a. The XPS spectra in Figure S3b show that doping was successful, as evidenced by the increased oxidation state of PEDOT. Quantifying the optical transmittance of the composite films was performed using UV-Vis spectroscopy with a PEDOT-graphene film and a graphene-only control. The transparencies of graphene and

PEDOT–graphene were approximately the same, at 76% and 75%, respectively, over the visible range, as shown in Figure 2C. These films can be used in applications in which transparency is essential.

Li et al. established a linear relationship between VPP PEDOT film thickness and transmittance for thicknesses in the range of 10 to 50 nm.[20] A control PEDOT film was analyzed, and the transmittance in the visible range was measured to be 93.7%. This value was used with the published data to determine an approximate thickness of 23 nm. The thickness of a control graphene film was determined using the principle established by Nair et al. that each layer of graphene reduces the transmittance of white light by 2.3%.[42] Our graphene film exhibited a transmittance of 87.6% over the visible range, corresponding to a reduction of 12.4%. This reduction indicates the presence of 5 to 6 layered graphene, agreeing with the 2D peak shoulder intensity calculations. The interlayer spacing of graphite is ~0.335 nm[43], so the graphene film thickness was approximately 2 nm. This information provided a likely range of composite film thickness.

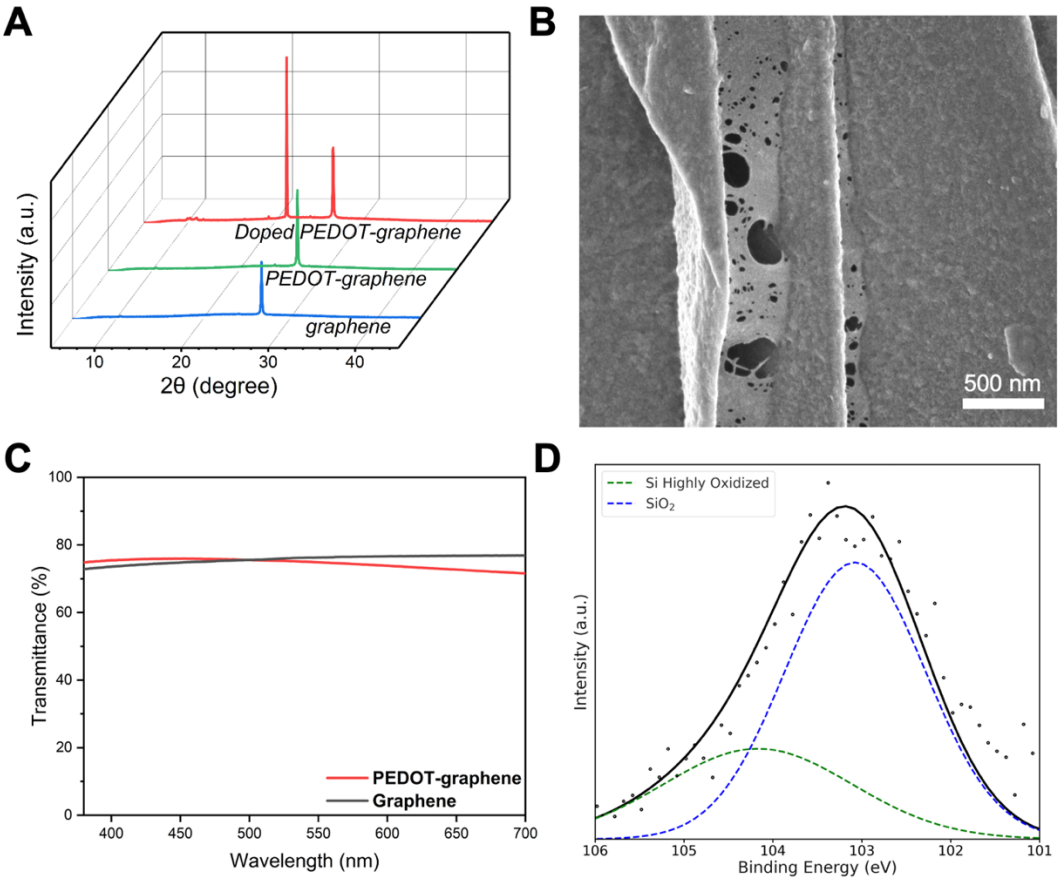

Figure 2. A) XRD spectra of a 300 µm graphene film (blue), a PEDOT–graphene film (green), and an acid-treated PEDOT–graphene film, also referred to as a doped film (red). B) SEM image of the PEDOT–graphene film. C) Transmittance of a film made of 300 µm flake natural graphite and transmittance of a PEDOT–graphene film produced from 300 µm flake graphite. D) XPS analysis of the Si 2p region. The plot displays experimental data (black circles) and fitted curves, originally deconvoluted with CasaXPS. The total fit (black solid line) is deconvoluted into two components: SiO_2 (blue dashed line) and highly oxidized Si (green dashed line).

XPS was also utilized as an approach to investigate the thickness of the PEDOT-graphene composite films. Figure 2D shows XPS peaks arising from the presence of SiO_2. The XPS peak resulting from Na in Figure S3C shows the SiO2 is a result of the underlying glass rather than environmental contamination. Because the XPS penetration depth is 10 nm or less, the thickness of the composite film must be less than 10 nm.[44] Based on this, the maximum thickness of 10 nm was determined. This value fit within the range predicted by the previous UV-vis studies. Using the conservative value of 10 nm for the composite film's thickness, the conductivity of our

PEDOT–graphene film was calculated to be, at minimum, 1070 S/cm. Table 1 compares this result to results in the literature.

As mentioned previously, the flake size of the graphite used in this study was larger than typically used with SITM. Our hypothesis was that larger graphene sheets would require fewer electron hopping events to conduct current than smaller flake-size sheets. We found that the largest flake size (300 μm) produced the most conductive films, but the smallest flake size (1 μm) produced the second most conductive films, as shown in Figure S4. This result arises from the observation that smaller flake-size graphite exfoliates faster.[45] Therefore, the extent of exfoliation and the size of the sheets comprising the film both play a role in the quality of the film. However, the smaller flake-size graphene is too small for the PEDOT to order itself correctly, resulting in a more amorphous PEDOT.

Having characterized our PEDOT-graphene films' structural and electrical properties, we next investigated their potential for sensing applications. During conductivity measurements, we observed the resistance of the films would significantly increase if someone were near the 4-point probe. Upon further investigation, it was observed that the films exhibited a specific response to human exhalation, manifested as an increase in electrical resistance.

Table 1. Conductivity comparison between transparent PEDOT thin films in literature

Semiconducting polymer	Conductivity (S/cm)	Carbon material used	Reference
PEDOT: PSS	7.172	Graphene quantum dots	46*
PEDOT: PSS	28	N/A	16
PEDOT: PSS	697.5	RTCVD graphene	18
PEDOT: PSS	757.6	Electrochemically exfoliated graphene	47
PEDOT	761	N/A	40*
PEDOT	960	N/A	20
PEDOT	1000	N/A	48*
PEDOT	1070	Pristine Graphene	This work

* Indicates that the transparency of the film was not clearly specified.

Based on these observations, we conducted various tests to investigate the film's response to different environmental factors, initially focusing on temperature as a potential stimulus. Accordingly, we placed the film in an oven at 100 °C for 10 min and saw no change in conductivity. Additionally, placing water on the film resulted in little to no response, suggesting that the response was due to a chemical in the breath. After testing several organic compounds, we found that triethylamine (TEA) had a significant effect, presumably due to the lone pair of electrons on nitrogen, which is known to interact with graphene and PEDOT in sensing applications.[11]

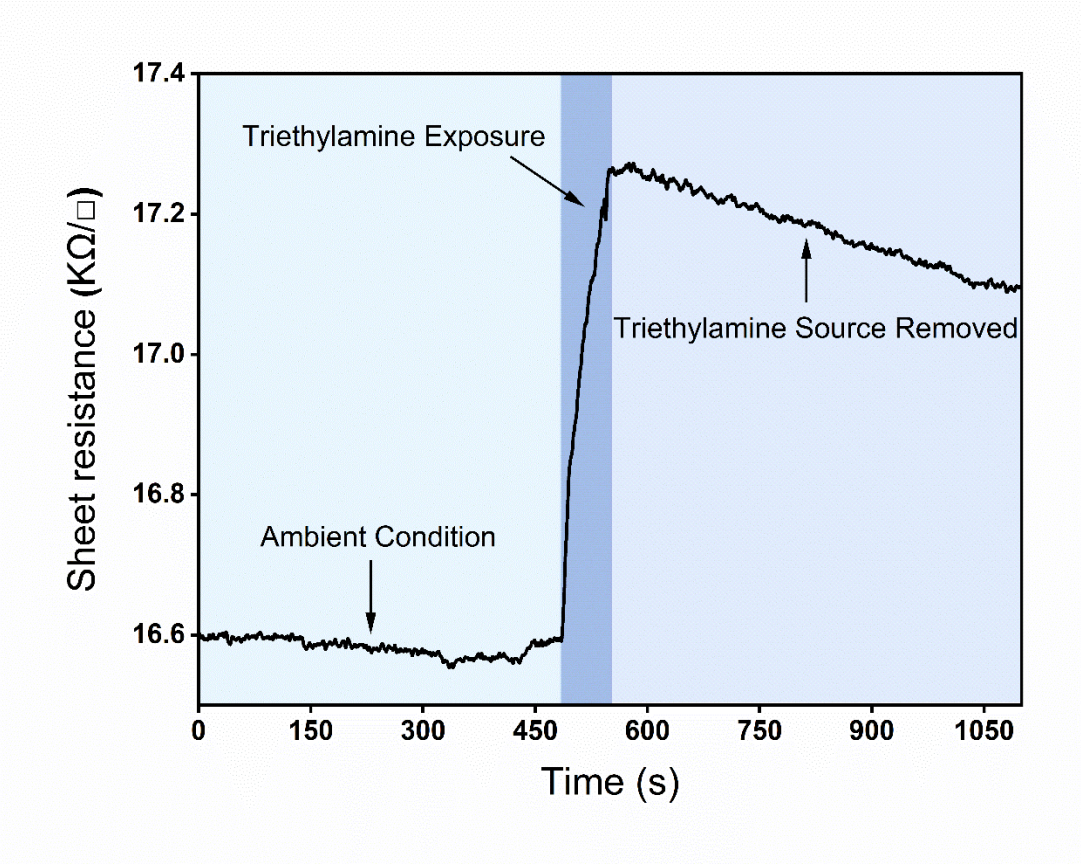

Figure 3. A sheet resistance vs. time plot for a PEDOT-graphene film being exposed to TEA.

As shown in Figure 3, when argon bubbled through TEA was blown on the film, the resistance sharply increased. However, the resistance decreased when the flow was removed. The recovery time was on the order of minutes. This was likely due to the nonporous nature of the film, as shown in the SEM image in Figure 2B. It should be noted that other solvents were tested, and responses to compounds such as acetone, heptane, ammonium hydroxide, and pyridine were observed. However, these responses exhibited lower specificity and longer recovery times, as seen in Figure S5. This response to amine gas suggests the film's applicability in sensing technologies.

CONCLUSIONS

In this study, we successfully developed a novel approach for the scalable production of highly conductive PEDOT-graphene films by utilizing a modified solvent interfacial trapping method (SITM) to exfoliate large-flake graphite. By employing overlapping graphene sheets as a template for vapor-phase polymerization (VPP) of EDOT, we achieved films with conductivities exceeding 1070 S/cm, surpassing those of comparable films previously reported. Our method circumvents the limitations associated with conventional methods, such as tip sonication and reducing oxidized graphene, thereby preserving the integrity and large lateral size of the graphene sheets.

Our results demonstrate that the larger graphite flake size contributed significantly to the conductivity of the films, presumably due to the reduced number of electron hopping events required for current conduction. The integration of graphene within the PEDOT matrix enhanced the electrical pathways and increased the crystallinity of the composite films, confirmed through various characterization techniques, including Raman spectroscopy, X-ray diffraction, and scanning electron microscopy. Additionally, the PEDOT-graphene films exhibited remarkable transparency (approximately 75%) and robustness, making them suitable candidates for applications in organic electronics. We further explored the potential of these films in sensing applications,

discovering a specific response to triethylamine (TEA) gas and highlighting their applicability in environmental monitoring and detection technologies.

Our approach presents a cost-effective and scalable method for producing high-performance PEDOT-graphene films that hold significant promise for replacing indium tin oxide (ITO) in various electronic devices. Future work will focus on optimizing the film properties for specific applications and exploring the integration of these films into commercial electronic devices. By overcoming the challenges of graphene production and enhancing the performance of PEDOT films, our study paves the way for the development of advanced materials that meet the demands of the rapidly evolving field of organic electronics

ASSOCIATED CONTENT

Supporting Information

The Supporting Information is available free of charge on the ACS Publications website.

Control XRD of the PEDOT film, Raman spectra of PEDOT: graphene films, XPS analysis, flake size effect on resistance, sensitivity to various stimuli (PDF).

AUTHOR INFORMATION

Corresponding Author

Douglas H. Adamson – Department of Chemistry, University of Connecticut, Storrs, Connecticut 06269, United States; Polymer Program, Institute of Materials Science, University of Connecticut, Storrs, Connecticut 06269, United States; orcid.org/0000-0002-7719-9287; Email: Adamson@uconn.edu

Authors

Sean T. Mcdermott – Polymer Program, Institute of Materials Science, University of Connecticut, Storrs, Connecticut 06269, United States; orcid.org/0000-0002-0669-9604
Brenden Ferland – Polymer Program, Institute of Materials Science, University of Connecticut, Storrs, Connecticut 06269, United States; orcid.org/0009-0008-6566-6088
Jinzhou Liu – Polymer Program, Institute of Materials Science, University of Connecticut, Storrs, Connecticut 06269, United States; orcid.org/0009-0002-0564-4502
Prabodha Abeykoon – Department of Chemistry, University of Connecticut, Storrs, Connecticut 06269, United States; orcid.org/0000-0002-8769-0803
Michael J. Joyce – Department of Chemistry, University of Connecticut, Storrs, Connecticut 06269, United States; orcid.org/0000-0002-3703-4656
Seth Shuster – Department of Chemistry, University of Connecticut, Storrs, Connecticut 06269, United States; orcid.org/0000-0002-8551-7417
Steven L. Suib – Departments of Chemistry, Chemical and Biomolecular Engineering, and Institute of Materials Science, University of Connecticut, Storrs, Connecticut 06269, United States; orcid.org/0000-0003-3073-311X

Funding Sources

This research was supported by NSF grant number 1535412.

ABBREVIATIONS

PEDOT, Poly(3,4-ethylenedioxythiophene); ITO, Indium Tin Oxide; CVD, Chemical Vapor Deposition; rGO, Reduced Graphene Oxide; NMP, N-Methyl-2-pyrrolidone; $Fe(OTs)_3$, iron(III)*p*-toluenesulfonate hexahydrate; SEM, Scanning Electron Microscopy; XRD, X-ray Diffraction; XPS, X-ray Photoelectron Spectroscopy; TEM, Transmission Electron Microscopy; UV-Vis, Ultraviolet-Visible; VPP, Vapor-Phase Polymerization; EDOT, 3,4-Ethylenedioxythiophene; SITM, Solvent Interface Trapping Method.

REFERENCES

(1) Angmo, D.; Krebs, F. C. Flexible ITO-Free Polymer Solar Cells. *J. Appl. Polym. Sci.* **2013**, *129* (1), 1–14. https://doi.org/10.1002/app.38854.

(2) Kirchmeyer, S.; Reuter, K. Scientific Importance, Properties and Growing Applications of Poly(3,4-Ethylenedioxythiophene). *J. Mater. Chem.* **2005**, *15* (21), 2077. https://doi.org/10.1039/b417803n.
(3) Paton, K. R.; Varrla, E.; Backes, C.; Smith, R. J.; Khan, U.; O'Neill, A.; Boland, C.; Lotya, M.; Istrate, O. M.; King, P.; Higgins, T.; Barwich, S.; May, P.; Puczkarski, P.; Ahmed, I.; Moebius, M.; Pettersson, H.; Long, E.; Coelho, J.; O'Brien, S. E.; McGuire, E. K.; Sanchez, B. M.; Duesberg, G. S.; McEvoy, N.; Pennycook, T. J.; Downing, C.; Crossley, A.; Nicolosi, V.; Coleman, J. N. Scalable Production of Large Quantities of Defect-Free Few-Layer Graphene by Shear Exfoliation in Liquids. *Nat. Mater.* **2014**, *13* (6), 624–630. https://doi.org/10.1038/nmat3944.
(4) Dierking, I. Carbon Allotropes as ITO Electrode Replacement Materials in Liquid Crystal Devices. *C* **2020**, *6* (4), 80. https://doi.org/10.3390/c6040080.
(5) Soni, M.; Bhattacharjee, M.; Ntagios, M.; Dahiya, R. Printed Temperature Sensor Based on PEDOT: PSS-Graphene Oxide Composite. *IEEE Sens. J.* **2020**, *20* (14), 7525–7531. https://doi.org/10.1109/JSEN.2020.2969667.
(6) Park, H.; Brown, P. R.; Bulović, V.; Kong, J. Graphene as Transparent Conducting Electrodes in Organic Photovoltaics: Studies in Graphene Morphology, Hole Transporting Layers, and Counter Electrodes. *Nano Lett.* **2012**, *12*, 133–140. https://doi.org/10.1021/nl2029859.
(7) Seekaew, Y.; Lokavee, S.; Phokharatkul, D.; Wisitsoraat, A.; Kerdcharoen, T.; Wongchoosuk, C. Low-Cost and Flexible Printed Graphene–PEDOT:PSS Gas Sensor for Ammonia Detection. *Org. Electron.* **2014**, *15* (11), 2971–2981. https://doi.org/10.1016/j.orgel.2014.08.044.
(8) Cho, E.-C.; Chang-Jian, C.-W.; Syu, W.-L.; Tseng, H.-S.; Lee, K.-C.; Huang, J.-H.; Hsiao, Y.-S. PEDOT-Modified Laser-Scribed Graphene Films as Bginder– and Metallic Current Collector–Free Electrodes for Large-Sized Supercapacitors. *Appl. Surf. Sci.* **2020**, *518*, 146193. https://doi.org/10.1016/j.apsusc.2020.146193.
(9) Redondo-Obispo, C.; Ripolles, T. S.; Cortijo-Campos, S.; Álvarez, A. L.; Climent-Pascual, E.; de Andrés, A.; Coya, C. Enhanced Stability and Efficiency in Inverted Perovskite Solar Cells through Graphene Doping of PEDOT:PSS Hole Transport Layer. *Mater. Des.* **2020**, *191*, 108587. https://doi.org/10.1016/j.matdes.2020.108587.
(10) Ko, S. H.; Kim, S. W.; Lee, Y. J. Flexible Sensor with Electrophoretic Polymerized Graphene Oxide/PEDOT:PSS Composite for Voltammetric Determination of Dopamine Concentration. *Sci. Rep.* **2021**, *11* (1), 21101. https://doi.org/10.1038/s41598-021-00712-w.
(11) Yang, Y.; Yang, X.; Yang, W.; Li, S.; Xu, J.; Jiang, Y. Porous Conducting Polymer and Reduced Graphene Oxide Nanocomposites for Room Temperature Gas Detection. *RSC Adv.* **2014**, *4* (80), 42546–42553. https://doi.org/10.1039/C4RA06560C.
(12) Vuorinen, T.; Niittynen, J.; Kankkunen, T.; Kraft, T. M.; Mäntysalo, M. Inkjet-Printed Graphene/PEDOT:PSS Temperature Sensors on a Skin-Conformable Polyurethane Substrate. *Sci. Rep.* **2016**, *6* (1), 35289. https://doi.org/10.1038/srep35289.
(13) Kim, D.; Zozoulenko, I. Why Is Pristine PEDOT Oxidized to 33%? A Density Functional Theory Study of Oxidative Polymerization Mechanism. *J. Phys. Chem. B* **2019**, *123* (24), 5160–5167. https://doi.org/10.1021/acs.jpcb.9b01745.
(14) Wen, Y.; Xu, J. Scientific Importance of Water-Processable PEDOT-PSS and Preparation, Challenge and New Application in Sensors of Its Film Electrode: A Review. *J. Polym. Sci. Part Polym. Chem.* **2017**, *55* (7), 1121–1150. https://doi.org/10.1002/pola.28482.
(15) Kim, J. Y.; Jung, J. H.; Lee, D. E.; Joo, J. Enhancement of Electrical Conductivity of Poly(3,4-Ethylenedioxythiophene)/Poly(4-Styrenesulfonate) by a Change of Solvents. *Synth. Met.* **2002**, *126* (2–3), 311–316. https://doi.org/10.1016/S0379-6779(01)00576-8.
(16) Barpuzary, D.; Kim, K.; Park, M. J. Two-Dimensional Growth of Large-Area Conjugated Polymers on Ice Surfaces: High Conductivity and Photoelectrochemical Applications. *ACS Nano* **2019**, *13* (4), 3953–3963. https://doi.org/10.1021/acsnano.8b07294.
(17) Skorenko, K. H.; Faucett, A. C.; Liu, J.; Ravvin, N. A.; Bernier, W. E.; Mativetsky, J. M.; Jones, W. E. Vapor Phase Polymerization and Mechanical Testing of Highly Electrically Conductive Poly(3,4-Ethylenedioxythiophene) for Flexible Devices. *Synth. Met.* **2015**, *209*, 297–303. https://doi.org/10.1016/j.synthmet.2015.07.033.
(18) Park, C.; Yoo, D.; Im, S.; Kim, S.; Cho, W.; Ryu, J.; Kim, J. H. Large-Scalable RTCVD Graphene/PEDOT:PSS Hybrid Conductive Film for Application in Transparent and Flexible Thermoelectric Nanogenerators. *RSC Adv.* **2017**, *7* (41), 25237–25243. https://doi.org/10.1039/C7RA02980B.
(19) Xia, Y.; Ouyang, J. Significant Conductivity Enhancement of Conductive Poly(3,4-Ethylenedioxythiophene): Poly(Styrenesulfonate) Films through a Treatment with Organic Carboxylic Acids and Inorganic Acids. *ACS Appl. Mater. Interfaces* **2010**, *2* (2), 474–483. https://doi.org/10.1021/am900708x.
(20) Li, B.; Skorenko, K. H.; Qiu, H.; Mativetsky, J. M.; Dwyer, D. B.; Bernier, W. E.; Jones, W. E. Effects of Interfacial Modification for Vapor Phase Polymerized PEDOT on Glass Substrate. *Synth. Met.* **2020**, *260*, 116293. https://doi.org/10.1016/j.synthmet.2020.116293.
(21) Novoselov, K. S.; Geim, A. K.; Morozov, S. V.; Jiang, D.; Zhang, Y.; Dubonos, S. V.; Grigorieva, I. V.; Firsov, A. A. Electric Field Effect in Atomically Thin Carbon Films. *Science* **2004**, *306* (5696), 666–669. https://doi.org/10.1126/science.1102896.
(22) Li, X.; Cai, W.; An, J.; Kim, S.; Nah, J.; Yang, D.; Piner, R.; Velamakanni, A.; Jung, I.; Tutuc, E.; Banerjee, S. K.; Colombo, L.; Ruoff, R. S. Large-Area Synthesis of High-Quality and Uniform Graphene Films on Copper Foils. *Science* **2009**, *324* (5932), 1312–1314. https://doi.org/10.1126/science.1171245.

(23) Barkan, T. Graphene: The Hype versus Commercial Reality. *Nat. Nanotechnol.* **2019**, *14* (10), 904–906. https://doi.org/10.1038/s41565-019-0556-1.
(24) Synthesis, G.; Saeed, M.; Alshammari, Y.; Majeed, S. A. Chemical Vapour Deposition of Graphene Synthesis, Characterisation, Adn Application: A Review. *Molecules* **2020**, *25* (3856), 2–62.
(25) Geim, a K.; Novoselov, K. S. The Rise of Graphene. *Nat. Mater.* **2007**, *6* (3), 183–191. https://doi.org/10.1038/nmat1849.
(26) Wang, L.; Lu, X.; Lei, S.; Song, Y. Graphene-Based Polyaniline Nanocomposites: Preparation, Properties and Applications. *J Mater Chem A* **2014**, *2* (13), 4491–4509. https://doi.org/10.1039/C3TA13462H.
(27) Wang, W.; Zhang, Q.; Li, J.; Liu, X.; Wang, L.; Zhu, J.; Luo, W.; Jiang, W. An Efficient Thermoelectric Material: Preparation of Reduced Graphene Oxide/Polyaniline Hybrid Composites by Cryogenic Grinding. *RSC Adv.* **2015**, *5* (12), 8988–8995. https://doi.org/10.1039/C4RA12051E.
(28) Cai, X.; Jiang, Z.; Zhang, X.; Zhang, X. Effects of Tip Sonication Parameters on Liquid Phase Exfoliation of Graphite into Graphene Nanoplatelets. *Nanoscale Res. Lett.* **2018**, *13* (1), 241. https://doi.org/10.1186/s11671-018-2648-5.
(29) Khan, U.; Porwal, H.; O'Neill, A.; Nawaz, K.; May, P.; Coleman, J. N. Solvent-Exfoliated Graphene at Extremely High Concentration. *Langmuir* **2011**, *27* (15), 9077–9082. https://doi.org/10.1021/la201797h.
(30) Barroso-Bujans, F.; Fernandez-Alonso, F.; Pomposo, J. A.; Cerveny, S.; Alegría, A.; Colmenero, J. Macromolecular Structure and Vibrational Dynamics of Confined Poly(Ethylene Oxide): From Subnanometer 2D-Intercalation into Graphite Oxide to Surface Adsorption onto Graphene Sheets. *ACS Macro Lett.* **2012**, *1* (5), 550–554. https://doi.org/10.1021/mz3001012.
(31) Alaferdov, A. V.; Savu, R.; Canesqui, M. A.; Kopelevich, Y. V.; da Silva, R. R.; Rozhkova, N. N.; Pavlov, D. A.; Usov, Yu. V.; de Trindade, G. M.; Moshkalev, S. A. Ripplocation in Graphite Nanoplatelets during Sonication Assisted Liquid Phase Exfoliation. *Carbon* **2018**, *129*, 826–829. https://doi.org/10.1016/j.carbon.2017.12.100.
(32) Bracamonte, M. V.; Lacconi, G. I.; Urreta, S. E.; Foa Torres, L. E. F. On the Nature of Defects in Liquid-Phase Exfoliated Graphene. *J. Phys. Chem. C* **2014**, *118* (28), 15455–15459. https://doi.org/10.1021/jp501930a.
(33) Das, S. K.; Gawas, R.; Chakrabarty, S.; Harini, G.; Patidar, R.; Jasuja, K. An Unexpected Transformation of Organic Solvents into 2D Fluorescent Quantum Dots during Ultrasonication-Assisted Liquid-Phase Exfoliation. *J. Phys. Chem. C* **2019**, *123* (41), 25412–25421. https://doi.org/10.1021/acs.jpcc.9b03975.
(34) Woltornist, S. J.; Oyer, A. J.; Carrillo, J.-M. Y.; Dobrynin, A. V.; Adamson, D. H. Conductive Thin Films of Pristine Graphene by Solvent Interface Trapping. *ACS Nano* **2013**, *7* (8), 7062–7066. https://doi.org/10.1021/nn402371c.
(35) Woltornist, S. J.; Carrillo, J.-M. Y.; Xu, T. O.; Dobrynin, A. V.; Adamson, D. H. Polymer/Pristine Graphene Based Composites: From Emulsions to Strong, Electrically Conducting Foams. *Macromolecules* **2015**, *48* (3), 687–693. https://doi.org/10.1021/ma5024236.
(36) Wang, Z.; Liang, H.; Adamson, D. H.; Dobrynin, A. V. From Graphene-like Sheet Stabilized Emulsions to Composite Polymeric Foams: Molecular Dynamics Simulations. *Macromolecules* **2018**, *51* (18), 7360–7367. https://doi.org/10.1021/acs.macromol.8b01082.
(37) Brown, E. E. B.; Woltornist, S. J.; Adamson, D. H. PolyHIPE Foams from Pristine Graphene: Strong, Porous, and Electrically Conductive Materials Templated by a 2D Surfactant. *J. Colloid Interface Sci.* **2020**, *580*, 700–708. https://doi.org/10.1016/j.jcis.2020.07.026.
(38) Hui, T.; Adamson, D. H. Kinetic Study of Surfactant-Free Graphene Exfoliation at a Solvent Interface. *Carbon* **2020**, *168*, 354–361. https://doi.org/10.1016/j.carbon.2020.06.043.
(39) Franco-Gonzalez, J. F.; Zozoulenko, I. V. Molecular Dynamics Study of Morphology of Doped PEDOT: From Solution to Dry Phase. *J. Phys. Chem. B* **2017**, *121* (16), 4299–4307. https://doi.org/10.1021/acs.jpcb.7b01510.
(40) Zuber, K.; Fabretto, M.; Hall, C.; Murphy, P. Improved PEDOT Conductivity via Suppression of Crystallite Formation in Fe(III) Tosylate During Vapor Phase Polymerization. *Macromol. Rapid Commun.* **2008**, *29* (18), 1503–1508. https://doi.org/10.1002/marc.200800325.
(41) Wang, X.; Zhang, X.; Sun, L.; Lee, D.; Lee, S.; Wang, M.; Zhao, J.; Shao-Horn, Y.; Dincă, M.; Palacios, T.; Gleason, K. K. High Electrical Conductivity and Carrier Mobility in oCVD PEDOT Thin Films by Engineered Crystallization and Acid Treatment. *Sci. Adv.* **2018**, *4* (9), eaat5780. https://doi.org/10.1126/sciadv.aat5780.
(42) Nair, R. R.; Blake, P.; Grigorenko, A. N.; Novoselov, K. S.; Booth, T. J.; Stauber, T.; Peres, N. M. R.; Geim, A. K. Fine Structure Constant Defines Visual Transparency of Graphene. *Science* **2008**, *320* (5881), 1308–1308. https://doi.org/10.1126/science.1156965.
(43) Ghosh, C.; Singh, M. K.; Parida, S.; Janish, M. T.; Dobley, A.; Dongare, A. M.; Carter, C. B. Phase Evolution and Structural Modulation during in Situ Lithiation of MoS2, WS2 and Graphite in TEM. *Sci. Rep.* **2021**, *11* (1), 9014. https://doi.org/10.1038/s41598-021-88395-1.
(44) Leng, Y. *Materials Characterization: Introduction to Microscopic and Spectroscopic Methods*, 1st ed.; Wiley, 2013. https://doi.org/10.1002/9783527670772.
(45) Hui, T.; Adamson, D. H. Kinetic Study of Surfactant-Free Graphene Exfoliation at a Solvent Interface. *Carbon* **2020**, *168*, 354–361. https://doi.org/10.1016/j.carbon.2020.06.043.
(46) Du, F.-P.; Cao, N.-N.; Zhang, Y.-F.; Fu, P.; Wu, Y.-G.; Lin, Z.-D.; Shi, R.; Amini, A.; Cheng, C. PEDOT:PSS/Graphene Quantum Dots Films with Enhanced Thermoelectric Properties via Strong Interfacial Interaction and Phase Separation. *Sci. Rep.* **2018**, *8* (1), 6441. https://doi.org/10.1038/s41598-018-24632-4.

(47) Liu, Z.; Parvez, K.; Li, R.; Dong, R.; Feng, X.; Müllen, K. Transparent Conductive Electrodes from Graphene/PEDOT:PSS Hybrid Inks for Ultrathin Organic Photodetectors. *Adv. Mater.* **2015**, *27* (4), 669–675. https://doi.org/10.1002/adma.201403826.
(48) Winther-Jensen, B.; Breiby, D. W.; West, K. Base Inhibited Oxidative Polymerization of 3,4-Ethylenedioxythiophene with Iron(III)Tosylate. *Synth. Met.* **2005**, *152* (1–3), 1–4. https://doi.org/10.1016/j.synthmet.2005.07.085.